UCRL--95973

DE87 011549

Gas-Cooled Reactor For Space Power Systems

Carl E. Walter
John S. Pearson

This paper was prepared for submittal t
1987 Intersociety Energy
Conversion Engineering Conference
Philadelphia, PA
August 10-14, 1987

May 1987

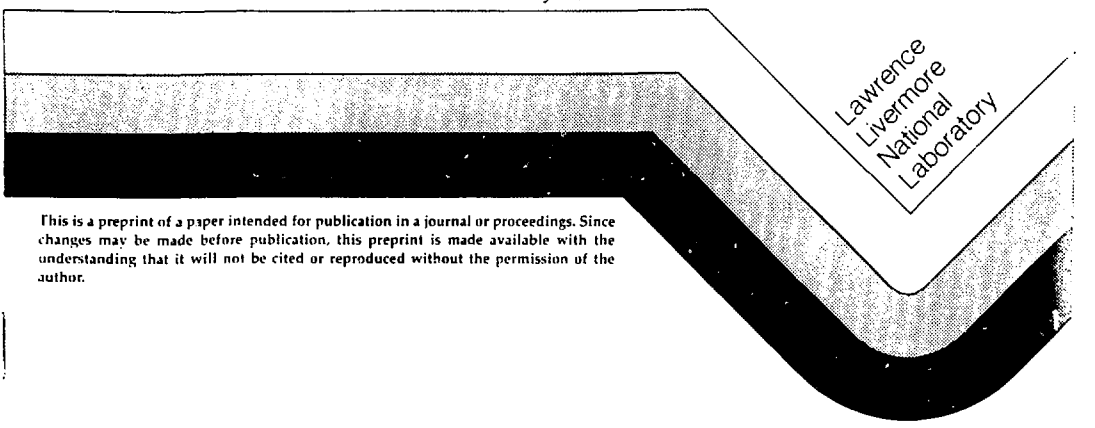

GAS-COOLED REACTOR FOR SPACE POWER SYSTEMS

Carl E. Walter and John S. Pearson
Lawrence Livermore National Laboratory
Livermore, CA

Abstract

Reactor characteristics based on extensive development work on the 500-MWt reactor for the Pluto nuclear ramjet are described for space power systems useful in the range of 2 to 20 MWe for operating times of 1 y. The modest pressure drop through the prismatic ceramic core is supported at the outlet end by a ceramic dome which also serves as a neutron reflector. Three core materials are considered which are useful at temperatures up to about 2000 K. Most of the calculations are based on a beryllium oxide with uranium dioxide core. Reactor control is accomplished by use of a burnable poison, a variable-leakage reflector, and internal control rods. Reactivity swings of 20% are obtained with a dozen internal boron-10 rods for the size cores studied. Criticality calculations were performed using the ALICE Monte Carlo code. The inherent high-temperature capability of the reactor design removes the reactor as a limiting condition on system performance. The low fuel inventories required, particularly for beryllium oxide reactors, make space power systems based on gas-cooled near-thermal reactors a lesser safeguard risk than those based on fast reactors.

Background

Large amounts of electric power are required for some systems envisioned in support of the nation's strategic defense. Since various applications are being considered, and an overall strategic defense power architecture study has not been completed, the required power levels and corresponding operating times for specific systems are not known. Arbitrarily, we chose to study a 50 MW reactor operating for 1 y. Such a reactor coupled with a Brayton cycle power conversion system could provide 10-15 MWe in space.

The reactor design described here benefits from earlier analyses of nuclear space power systems conducted at our Laboratory. Both gas-and-liquid-cooled reactors were considered at that time. We selected for further study a gas-cooled reactor design with a Brayton cycle. The reactor design draws heavily on the extensive development experience with the 500-MWt reactor for the Pluto nuclear ramjet shown in Fig. 1. That development culminated in a successful full-power ground test. [1,2]

Gas-cooled reactors, are generally thermal or epithermal reactors and are well suited for space power applications. They may be designed for core power densities comparable to those found in fast reactors. Allowable fuel burnup constrains core power density in a fast reactor but not in a thermal or epithermal reactor. Another comparison may be made of the mass of fissionable material and the operating flux in fast and epithermal reactors. Fig. 2 shows this relationship for reactors operating for 1 y at 50 MW. In the best case, the initial mass of U-235 for a 10%-burnup fast reactor core is about three times as much as for an epithermal reactor, while the effective neutron flux (higher median fission energy in the case of the fast reactor) is an order of magnitude higher. These relationships imply that epithermal reactors are a lower safeguard risk and can be used with a lighter radiation shield than fast reactors. The goal of this study is to characterize the neutronic, thermal, and mechanical attributes of a reactor suitable for use in a space power system.

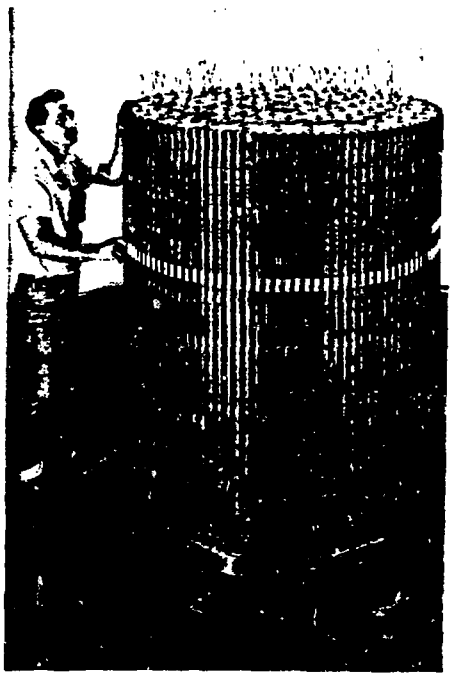

Fig. 1. The Tory II-C reactor was designed and tested for the Pluto ramjet application. The partially assembled Tory II-C reactor shown here was 1.4 m in diameter by 1.6 m high.

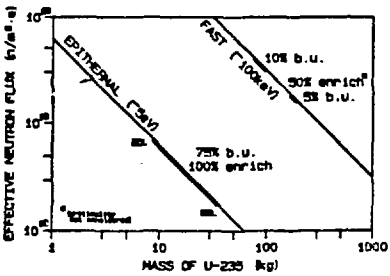

Fig. 2. Epithermal reactors operate at lower neutron flux, require a lower fuel inventory, and can sustain higher burn-up than fast reactors. These data are for reactors operating for 1 y at 50 MW.

Space Power System

Once safety features of the reactor system are assured, an overriding design consideration in space power systems is reduction of their mass. Since power conversion systems convert heat energy to work (electric power), Carnot principles apply. A real thermodynamic power conversion cycle cannot be more efficient than a Carnot cycle whose efficiency is equal to $(1 - T_2/T_1)$ where T_2 is the sink temperature (related to the radiator temperature in this case) and T_1 is the temperature of the heat source (reactor coolant exit temperature).

Since the radiator represents a large fraction of the mass of a space power system (increasingly so as power increases), to reduce system mass, the radiator should be allowed to operate at a high temperature. While a lower design radiator temperature, T_2, would result in a more efficient system, system mass increases considerably. The area of the radiator, and hence its mass varies inversely with the fourth power of temperature, and significant area/mass savings result for small increases in radiator temperature. This places a premium on a high temperature (T_1), heat source, particularly for systems in which the working fluid is a gas. Thermodynamic gas cycles have variable temperature radiators which tend to be large. We have concentrated on the design of all-ceramic reactors which operate at a high temperature (T_1) for use with Brayton cycles.

In establishing the condition of operation required for the reactor, we considered four thermodynamic cases. These were indirect Brayton cycles with and without a regenerator in the power conversion loop (Cases 1 and 2, respectively) and direct Brayton cycles with and without a regenerator (Cases 3 and 4, respectively). All four cases have their equipment arranged in a conical configuration. Heat is rejected from the power conversion loop by direct contact of the working gas with heat pipes. Use of a more advanced radiator design would significantly lower system specific mass.

We used conventional equations and correlations to determine system performance. We modeled each system component to determine its mass as a function of relevant system parameters, such as temperature, pressure and working fluid. We used a computer code called AD [3] to solve simultaneously the many resulting equations for various combinations of cycle temperatures and turbine pressure ratios. The equation solver is then used near the "optimum" values of these ratios to evaluate the sensitivity of selected parameters in the equations.

Models for the power conversion unit, shield, radiator, and connecting piping were general; however, the heat exchangers and the reactor models were more detailed. Power conversion components and the associated piping were modularized to provide, for example, four or six parallel sets between the reactor and the radiator.

We prescribed specific mass coefficients for the turbine (0.1 kg/kW), compressor (0.15 kg/kW), and alternator (0.2 kg/kW). The output power of each device is multiplied by the above coefficients to obtain their individual masses. The specific mass coefficient for the turbine-compressors-alternator unit is then calculated by summing the contributions for the three components and dividing the sum by the output electric power. Typical values of this coefficient are in general agreement with published data.

Since mission requirements are uncertain, a shadow shield of lithium hydride 0.5-m thick is located close to the reactor. The shield provides neutron attenuation of approximately 10^{-6} in its conical shadow. No consideration was given to gamma attenuation. When that requirement is known, effective placement of power conversion components and heat exchangers can contribute to the gamma shield design. The effect of cone angle on system mass was also studied.

The heat pipe radiator incorporated in the model has a specific mass [4] of 20 kg/m². Designs for much lighter radiators have been proposed, but their feasibility is not certain. The heat pipe radiator design is sufficiently redundant to survive meteoroid damage. We also assume that structural, rather than meteoroid considerations determine piping and pressure vessel thicknesses. The working fluid pressure drop is fixed at 5% of the inlet pressure to the radiator, and the radiator surface temperature is assumed to be 50 K lower than the working fluid temperature at all points in the radiator.

We modeled the effect of connecting piping on mass and performance. Heat exchangers of the compact counter-flow design in three of the cases were evaluated, either as a regenerator or as means of transferring heat from the reactor loop to the turbine loop. Structural material strength was expressed by a single equation based on published or projected data of 1% creep stress/density ratio for a series of increasingly refractory alloys. Explicit

density values are needed only to determine material thickness, since pressure vessel and pipe masses are determined by the stress/density ratio of the materials, not the density alone.

We obtained a large amount of data from computations using the system models developed for the four cases. Results are summarized in Table 1. Considerably more information could be obtained from further computations directed toward achieving more optimum situations, and toward quantifying the sensitivity of salient characteristics, such as mass and efficiency, to changes in "fixed" parameters.

Table 1. Summary of the principal performance and mass characteristics of the cases studied. Turbine inlet temperature is 1600 K in all cases. The reactor outlet temperature is 1625 K in cases 1 and 2.

	INDIRECT-REGENERATED	INDIRECT	DIRECT-REGENERATED						DIRECT	
Case	1	2	3a	3b	3c	3c[b]	3d	4a	4b	
P_max (MPa)	10	10	10	10	10	10	20	10	2	
Cycle efficiency (%)	33	19	37	37	32	33	29	29	14	
Reactor flowrate (kg/s)	19	16	14	11	12	15	32	11	4	
Specific mass (kg/MW)	18.3	16.7	6.4	6.9	6.2	5.8	6.8	7.7	7.9	
Turbine press ratio	1.8	2.4	1.8	2.4	2.4	1.8	2.0	2.2	2.2	
Min cycle temp (K)	860	600	600	600	600	860	860	600	475	
Circulator[c]	1	neg	—	—	—	—	—	—	—	
Intermed Heat Exch[c]	3	3	—	—	—	—	—	—	—	
Piping[c]	2	1	2	4	4	2	2	2	0	
Reactor[c]	2	2	3	3	3	3	3	2	12	
Shield[c]	3	3	4	5	5	4	2	4	21	
Turb/Comp/Alt[c]	7	8	7	10	12	8	12	8	13	
Regenerator[c]	12	—	14[b]	8	6	7	8	—	—	
Radiator[c]	70	86	70	74	69	77	78	86	45	

a. Helium/xenon working fluid
b. For true optimum
c. Component mass contributions (%) to total system mass

In general, we performed our computations for 10-MWe systems using helium as the reactor coolant/working fluid. But some variations are included in Table 1. Cases 3e and 4b represent 20-MWe and 2-MWe systems, respectively. Case 3d uses helium/xenon working fluid and should be compared with Case 3a, which uses pure helium for identical fixed cycle conditions (maximum and minimum temperatures, maximum pressure, turbine pressure ratio). Cases 3b and 3c differ only in their minimum cycle temperatures. None of the cases summarized here has been truly optimized for minimum system specific mass. Since the same reactor is used in each case, clearly the reactor is "oversize" even for the highest reactor power core (Case 3e), where the core power density is only 170 MW/m³. Except for Case 4b, a reasonable savings in reactor mass would not lower the system mass significantly. It does not seem prudent under these conditions to reduce the reactor size and incur penalties of higher fuel inventory and higher reactor pressure drop.

While further effort is needed to optimize these cases, Table 1 shows that the direct-regenerated cycle configuration (Case 3c) at 10-MWe minimizes specific system mass and that the radiator contributes a major portion of the system mass. This system not only has low specific mass but is more efficient and thus requires a lower reactor fuel inventory. At the 2-MWe power level (Case 4c) the radiator no longer dominates system mass, and assumptions regarding other system components should be examined more closely. Final determination of reactor size and operating conditions should be made only when application requirements are well known.

An important consideration is the system operating pressure. A significant decrease in system mass results when operating pressure is increased. We did not increase system pressure above 5 MPa because we wanted to hold the thickness of the reactor pressure vessel below about 10 mm. Heavier sections in this critical component, if made from refractory alloys, may not be as reliable.

Comparison of pure helium and a mixture of helium and xenon having molecular weight equivalent to that of argon indicates a slight preference for pure helium, as shown in Cases 3a and 3d. At lower power levels, where the relative mass of the power conversion equipment is higher, a higher molecular weight gas with good conductivity may be preferred.

Since the radiator size appears to be extremely large for Brayton cycles at power levels of 10 MWe or above, it is appropriate to also consider integrating gas-cooled reactors with other power conversion methods. The mass of intermediate heat exchangers and circulators for the reactor loop is seen to be low (Table 1, Cases 1 and 2). Thus, it appears reasonable that a gas-to-liquid heat exchanger could be provided for a small mass penalty, which would be more than compensated by the mass savings of a radiator operating at a higher effective temperature.

Reactor Characteristics

The reactor, configured as shown in Fig. 3, has a prismatic ceramic core composed of several thousand "pencil shaped" tubes made from a homogeneous mixture of moderator and fuel. Radial compression forces exerted by girdle springs on the cylindrical surface of the core hold the tubes together. The reference core, 80-cm in diameter by 80-cm long, (referred to as an 80-cm size core), has a flow porosity of 30%. The reference core materials, also used in the Tory II-C (Pluto) reactor, are beryllium oxide and uranium dioxide ($BeO + UO_2$). The Tory II-C reactor core (diameter, 1.2 m; height, 1.3 m) is considerably larger than the reference core used in this study. In the present designs, a layer of zirconia insulation between the fueled core and the girdle springs allows the inlet reactor gas to cool the springs and the reactor pressure vessel before the gas flows through the core. Spring force requirements are minimal since maneuver loads, if any, are very

low, and gas pressure gradients are favorable. This may allow the springs and pressure vessel to be made from non-refractory metals. A ceramic dome at the outlet end, designed to experience only compressive stresses, supports the modest pressure drop through the core and also serves as a neutron reflector. Inlet and outlet reflectors are made from the same moderating material as is used in the core.

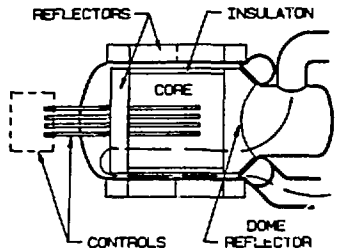

Fig. 3. The reactor consists of a ceramic core supported in a metal pressure vessel with an external movable radial reflector and internal control rods.

Control of thermal reactors made from the materials considered is accomplished by use of a burnable poison, a variable-leakage reflector, and internal control rods. The reactivity worths of these mechanisms are discussed in the next section.

Water immersion safety in the event of a launch accident is achieved with a number of hafnium wires passing through the core. Core thermal-hydraulic calculations indicate that exit Mach numbers less than 0.1 are required. The inert gas flow may be treated as incompressible, and no flow instability mechanisms have been found.

Several core material choices are possible. Besides BeO + UO_2, we evaluated boron carbide with uranium boride (B-11 isotope), and carbon with uranium dicarbide. These materials all provide a thermal or epithermal neutron spectrum in the sizes considered. Based on their volatilities, we estimate these material combinations to be useful at temperatures up to about 1950 K, 2000 K, and 2200 K, respectively. Higher temperatures could be achieved with appropriate coatings. For conservatism, we limited the reactor coolant exit temperature in this study to 1625 K. Our results show that, for a given reactor geometry, the choice of core material causes only a negligible difference in system mass. However, study and experimental work is required to quantify fission product retention and irradiation effects at high burnup for all three material choices.

The BeO + UO_2 oxide system is an outstanding candidate. This system is highly developed from the Pluto project, has good mechanical and physical properties, and results in the lowest critical mass (e.g. 8.7 kg at 1400 K for the reference core) for the same size and porosity reactor. A possible drawback (which needs to be evaluated more fully) is the extent to which the toxicity of beryllium oxide represents a hazard to the public in the event of a launch accident. The reactor we modeled is based on a beryllium oxide core.

Its anticipated structural, chemical, and thermal properties make the boron system a leading candidate for high burnup missions where a burnable poison (B-10) would be desirable. Sufficiently pure B-11 can be obtained at a reasonable cost with the desired amount of B-10 for reactivity control if the design operating life is sufficiently longer than one year.

As in the case of BeO + UO_2, the C + UC_2 is also highly developed (it was developed for nuclear rockets), has the highest operating temperature capability, and has excellent thermal stress characteristics. Multiple-hole fuel elements are more feasible in the carbon system, should that be desirable. The major disadvantage of the carbon system is its relatively high critical mass (e.g. 269 kg versus 44 kg for BeO in 68-cm diameter by 68-cm long cores having 30% flow porosity at 291 K). Nevertheless, all three material systems result in considerably lower fuel inventories than would be required for fast reactors.

Reactor Neutronics

The ALICE computer code [5,6] was used to make neutronics calculations. ALICE is a Monte Carlo neutron/photon transport code which uses the probability table method for handling multiband cross sections [7] and properly treats resonance self-shielding effects. The code has previously been compared with excellent agreement over a range of uranium enrichments against the Monte Carlo code MCNP which uses continuous energy cross sections [8]. In addition, two cases from the current study were independently run using MCNP [9] and yielded good agreement. (ALICE calculated k_{eff} values of 0.942 ± 0.005 for an unreflected core and 1.009 ± 0.005 for a reflected core; MCNP gave 0.938 ± 0.005 and 1.026 ± 0.005 for these cases respectively). The cross section sets used by ALICE were derived from the Lawrence Livermore National Laboratory Evaluated Nuclear Data Library, ENDL-86. One set of cross sections was used for "cold" calculations at 291 K. A set of "hot" cross sections was doppler broadened for 1400 K.

The standard model used for these calculations is shown in Fig. 4 for the reference 80-cm size core. Variations on this model were also run, as specified in the text. For an early set of survey calculations the axial reflector density was inadvertently held constant, but for subsequent calculations it was varied with the core porosity. For the three fuels considered (BeO+UO_2, B_4C+UB_4, and C+UC_2) the fuel number densities were calculated as a function of the core flow porosity (which was homogeneously distributed within the core) and the volume fraction of the fissile compound in the fuel.

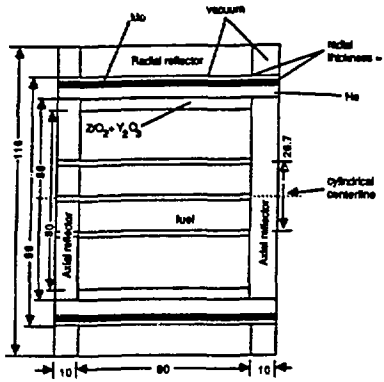

Fig. 4. Standard reactor model for the 80-cm size core at 291 K. One 1-cm diameter control rod is through the center, others are equally spaced at radius of 26.7 cm.

A criticality survey was made of the three fuels in a 68-cm size core as a function of core porosity between 0.20 and 0.35 (Table 2). A set of points was also determined for the C+UC_2 fuel in a 100-cm size core. For these calculations the axial reflector density was inadvertently held constant. The survey shows several significant effects. Varying the porosity in this size core strongly affects the mass of U-235 fuel required to achieve criticality. Increasing porosity requires more fuel to compensate. (This effect is even greater if the axial reflector porosity is varied with core porosity as shown by comparison to entries marked with an asterisk in the table.) The more porous reactors at this core size which require a higher fuel loading tend to be much faster reactors with a large increase in the median fission energy, $\bar{E}_f$. Also the C + UC_2 core has the highest median fission energy and requires much more uranium than the other two materials to achieve criticality for a corresponding porosity and core size.

A survey of critical masses is also shown in Table 3 for various core sizes between 68-cm and 100-cm at porosity 0.30 and 291 K. The critical mass decreases dramatically for the BeO + UO_2 and B_4C + UB_4 fuels as the median fission energy decreases with increasing core size. The 80-cm and 90-cm size cores for these materials have median fission energies in the thermal region, whereas the 68-cm core is critical in the intermediate energy range (between a few eV to 10 eV). The critical mass for the C + UC_2 core, however, varies little between the 68-cm and 100-cm size cores as the median fission energy remains quite high.

The neutron capture-to-fission ratio, α, is also lower in the larger BeO + UO_2 and B_4C + UB_4 critical cores which have lower critical mass. The capture-to-fission ratio is the ratio of the relative probability that the compound nucleus will decay by emission of capture gamma rays versus the probability of decay by fission. Since fuel consumption is proportional to $(1 + \alpha)$ this implies that less fuel burnup is required per unit of power produced in the larger, more thermal cores. Shown in Fig. 5 are the values of α for both BeO + UO_2 and B_4C + UB_4 cores in the 80-cm size core of porosity 0.30 at 291 K and 1400 K over a range of U-235 masses. The values of α all lie very close to a single smooth curve.

Table 2. Survey of critical points at 291 K as a function of porosity and core size. The axial reflector porosity matches the core porosity for cases marked by *. Reflector porosity was zero for other cases.

Fuel	Core Diameter (cm)	Porosity	k_{eff}	$\bar{E}_f$ (eV)	α	Mass of U-235 (kg)
B_4C+UB_4	68	0.20	0.997 ± 0.006	8.23		15.8
B_4C+UB_4	68	0.25	1.006 ± 0.010	86.7		38.3
B_4C+UB_4	68	0.30	1.006 ± 0.008	200		62.8
B_4C+UB_4	68	0.35	1.007 ± 0.008	407		113.5
BeO+UO_2	68	0.25	1.006 ± 0.008	8.017		8.96
BeO+UO_2	68	0.30	1.006 ± 0.007	8.75		24.4
BeO+UO_2	68	0.35	1.013 ± 0.008	83.9		57.3
C+UC_2	68	0.20	1.016 ± 0.010	8130		200
C+UC_2	68	0.25	0.987 ± 0.011	8170		225
C+UC_2	68	0.30	1.013 ± 0.012	18300		262
C+UC_2	100	0.20	0.994 ± 0.009	180		159
C+UC_2	100	0.25	1.003 ± 0.008	300		197
C+UC_2	100	0.30	0.995 ± 0.010	640		250
C+UC_2	100	0.35	0.993 ± 0.006	1240		295
B_4C+UB_4*	68	0.30	0.999 ± 0.006	340	8.44	102.5
BeO+UO_2*	68	0.30	0.998 ± 0.003	42.8	8.44	41.6
C+UC_2*	68	0.30	0.999 ± 0.005	20000		259
B_4C+UB_4*	80	0.30	1.002 ± 0.008	0.131	0.30	17.13
BeO+UO_2*	80	0.30	1.003 ± 0.009	0.017	0.23	3.97
B_4C+UB_4*	90	0.30	1.006 ± 0.008	0.016	0.20	4.57
BeO+UO_2*	90	0.30	0.996 ± 0.003	0.017	4.19	2.86

Table 3. Temperature effects between 291 K and 1400 K resulting from thermal expansion of the core and doppler broadened cross sections applied separately and together.

Fuel	Core Diameter (cm)	Cross-Section Temperature (K)	Thermal Expansion	$\bar{E}_f$ (eV)	k_{eff}
BeO+UO_2	68	291	No	42.8	0.998 ± 0.003
BeO+UO_2	68	1400	No	42.8	1.001 ± 0.003
BeO+UO_2	68	291	Yes	42.9	0.992 ± 0.003
BeO+UO_2	68	1400	Yes	42.4	0.985 ± 0.002
B_4C+UB_4	68	291	No	340	0.999 ± 0.005
B_4C+UB_4	68	1400	No	307	1.004 ± 0.003
B_4C+UB_4	68	291	Yes	302	0.994 ± 0.004
B_4C+UB_4	68	1400	Yes	306	0.998 ± 0.002
BeO+UO_2	90	291	No	0.017	0.996 ± 0.003
BeO+UO_2	90	1400	No	0.072	0.863 ± 0.004
B_4C+UB_4	90	291	No	0.016	1.009 ± 0.003
B_4C+UB_4	90	1400	No	0.070	0.888 ± 0.003

The thermal effects on reactivity are shown in Table 3 for the 68-cm and 90-cm size cores with BeO + UO_2 and B_4C + UB_4 fuels. The nuclear effect was tested using cross sections doppler broadened for 1400 K. The effect of thermal expansion was tested in a conservative way by expanding the core and axial reflector model,

but not the other reactor materials. Linear expansions of 0.60% for B_4C and 1.07% for BeO were used between 291 K and 1400 K. For the 68-cm core a small reduction in k_{eff} results from the material expansion, especially in the BeO + UO_2 core which has the larger linear expansion fraction. However, no clear conclusion can be drawn for the cross section effect of doppler broadening within the statistical uncertainties. Since both reactors have median fission energies of tens to hundreds of eV, one doesn't expect much effect from doppler broadening. However, the larger 90-cm size cores for both the B_4C + UB_4 and BeO + UO_2 fuels, which have thermal median fission energies, show a significant decrease (about 12-13%) in reactivity with rising temperature as a result of the doppler broadened cross sections at 1400 K.

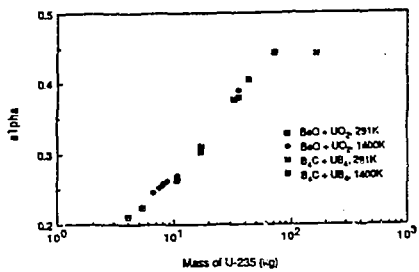

Fig. . The capture-to-fission ratio, α, plotted as a function of U-235 mass for the 80-cm size core of porosity 0.30.

We selected the reference core with BeO + UO_2 material, 80-cm size core, and flow porosity of 0.30. Table 4 lists various results. A consumption mass was added to the 1400 K critical mass to approximate the fuel required to produce 50 MWt of power for 1 y. The consumption mass, M_c, was calculated by: [10]

$$M_c = (895)\ (1 + \alpha)\ \frac{PA}{E_R}\ T = 26.7 \text{ kg}$$

where P is the power of 50 MW, T is one year, E_R is a recoverable energy of 200 MeV, A is the atomic mass of U-235, and the fission-to-capture ratio, α , was taken to be 0.39.

Table 4. Results for 80-cm cores with BeO+UO_2 fuel and porosity 0.30.

Mass of U-235 (kg)	Temperature (K)	Thermal Expansion	$\bar{E}_f$ (eV)	α	k_{eff}
3.97	291	No	0.017	0.21	1.003 ± 0.009
3.97	1400	No	0.070	0.23	0.916 ± 0.005
8.7	1400	Yes	0.076	0.26	0.997 ± 0.008
35.4	291	No	3.3	0.38	1.097 ± 0.005
35.4	1400	No	4.9	0.39	1.093 ± 0.005
35.4	1400	Yes	5.1	0.40	1.073 ± 0.005

The clean critical reactor (3.97 kg of U-235) is quite thermal with $\bar{E}_f$ of hundredths of an eV, and shows a decrease in reactivity (8%) with rising temperature (from 291 K to 1400 K) as a result of the doppler broadened cross sections. With the consumption mass added, the 35.4 kg U-235 reactor is much faster with $\bar{E}_f$ of several eV. The value of α also increased from about 0.26 to 0.40 with the additional fuel. The temperature effects from the doppler broadened cross sections are no longer measurable within statistics, although thermal expansion still results in a decrease in reactivity of 2%.

The reactivity worth of the control mechanisms (control rods and movable radial reflector) was studied for the 35.4 kg U-235 reactor. The radial reflector is worth 5%, reducing the value of k_{eff} at 291 K from 1.097 ± 0.005 to 1.045 ± 0.005 when fully open. The relative worths of fully inserting one, seven, twelve, or thirteen 1-cm diameter B-10 control rods are listed in Table 5. The rods are very effective with 12 rods worth about 20%, reducing k_{eff} to 0.891 ± 0.006. The effect on reactivity worth from varying the B-10 density of 12 control rods was studied. At 50% of normal B-10 density the rods are still nearly as effective as at full density, and at 20% density k_{eff} = 0.945 ± 0.007. The reactivity worth of inserting twelve B-10 control rods is also shown in Fig. 6 as a function of insertion length. A smooth curve results with the highest change in reactivity per change in insertion length occurring around the center of the core, as expected.

Table 5. The reactivity worth of 1-cm diameter B-10 control rods at 291 K for the 80-cm size BeO+UO_2 core with consumption fuel.

Number of Rods	$\bar{E}_f$ (eV)	α	k_{eff}
0	2.6	0.39	1.094 ± 0.007
1	5.0	0.38	1.079 ± 0.008
7	6.9	0.39	0.958 ± 0.006
12	7.5	0.39	0.891 ± 0.006
13	7.8	0.39	0.875 ± 0.007

The mass of either B-10 or Gd (natural) burnable poison was determined which would reduce the value of k_{eff} for a clean new reactor with consumption mass to about 1% above critical. Expressed as a weight percent of the core material, 0.003wt% of B-10 yielded k_{eff} = 1.010 ± 0.005 ($\bar{E}_f$ = 7.6 eV, α = 0.40), and 0.025 wt% of Gd yielded k_{eff} = 1.005 ± 0.006 ($\bar{E}_f$ = 7.7 eV, α = 0.40). Continuing calculations will determine burn-up characteristics and rates.

Two accident conditions were considered: a flooded reactor and a crushed reactor. The flooded reactor was modeled by replacing all voids (including the porosity) with water and closely reflecting the reactor externally by 20 cm of water. The water effectively moderates

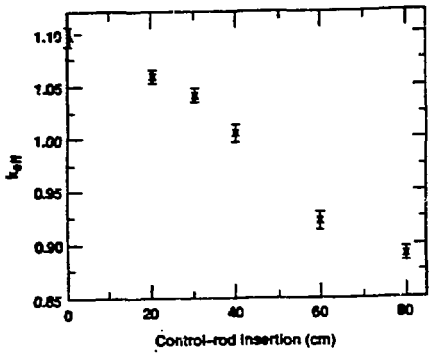

Fig. 6. Reactivity worth of twelve B-10 control rods as a function of insertion distance.

the neutrons in the core reducing $\bar{E}_f$ from 7.6 eV in the unflooded reactor to a very thermal value of 0.018 eV flooded. As a result, the reactor becomes supercritical (k_{eff} = 1.377 ± 0.007) even with the 0.003wt% B-10 burnable poison and twelve B-10 control rods inserted. The insertion of 2 mm diameter cadmium or hafnium wires in various fractions of the core flow passages was studied as a method to keep the flooded reactor subcritical. This was first modeled by homogenously mixing the wire poison material into the core (reactor model), although this probably under-estimates the reactivity because self-shielding effects are not included. Next an infinite planar array of fuel elements was modeled with wires explicitly modeled in a fraction of them. This probably over-estimates the reactivity because of the infinite array and because the control rods are not included. Thus, the actual reactivity should lie between the two models. The results (Fig. 7) indicate that putting cadmium or hafnium poison wires in more than 25% of the flow passages would poison the reactor sufficiently to keep it subcritical if flooded.

A radially crushed reactor was modeled by removing all voids (conservative) and close-packing the reactor materials. With the burnable B-10 poison and twelve B-10 control rods inserted, this unlikely accident only raised the reactivity to a slightly subcritical value of k_{eff} = 0.978 ± 0.007. The median fission energy of $\bar{E}_f$ = 7.7 eV was essentially unchanged from the corresponding undamaged reactor. Homogeneously mixing into the core the equivalent mass of 2 mm diameter cadmium wires in half the core holes significantly reduced the reactivity to k_{eff} = 0.519 ± 0.010. Thus, the crushed reactor is a much less severe accident than the flooded reactor, but neither would cause a supercritical condition with an adequate number of poison wires inserted into the core.

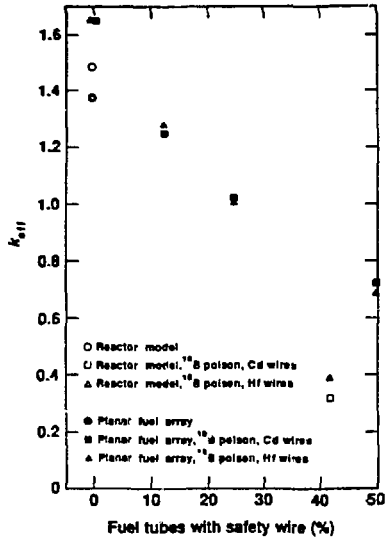

Fig. 7. Effect on reactivity of inserting 2 mm diameter cadmium or hafnium poison wires into fuel rod flow passages.

Conclusions

Although this was an abbreviated study, general conclusions may be stated. Gas-cooled thermal reactors permit high-temperature power conversion and appear to provide reasonable multi-megawatt space power systems. The inherent high-temperature capability of the reactor design considered removes reactor technology as a limiting condition on system operating temperature. The low fuel inventories required, particularly for BeO + UO_2 reactors, make space power systems based on gas-cooled near-thermal reactors a lesser safeguard risk than those based on fast reactors. In particular:

- BeO-moderated, gas-cooled reactors appear suitable for space power applications.
- A database exists for reactors of this design.
- Only one reactor need be developed for applications in this power range.
- Because of its high-temperature capability, low mass, and low fuel inventory, this reactor design coupled with a compact heat exchanger should also be considered with other means of power conversion.
- The reactor remains safe even if fully immersed in water or is crushed in an accident.

Acknowledgments

This work was performed under the auspices of the U.S. Department of Energy by Lawrence Livermore National Laboratory under Contract W-7405-Eng-48. We gratefully acknowledge technical discussions and assistance from several people, most notably C.S. Barnett, D.O. Blackketter, F.A. Kloverstrom, E.F. Plechaty and P. B. Mohr.

References

1. Walter, C. E., Ed. (1964) Engineering Design of the Tory II-C Nuclear Ramjet Reactor, UCRL-7679, Lawrence Livermore National Laboratory, Livermore, CA.

2. Reynolds, H. L., Ed. (1964) Tory II-C Reactor Test Report, UCRL-12069, Lawrence Livermore National Laboratory, Livermore, CA.

3. Blackketter, D. O. (1986) Unpublished Results, California State University, Chico, CA.

4. Prenger, F. C. and J. A. Sullivan (1982) Conceptual Designs for 100 MW Space Radiators, LAUR 82-3279, Los Alamos Scientific Laboratory, Los Alamos, NM.

5. Plechaty, E. F. and J. R. Kimlinger (1976) TARNP: A Coupled Neutron-photon Monte Carlo Transport Code, UCRL-50400, Vol. 14, Lawrence Livermore National Laboratory, Livermore, CA.

6. Kimlinger, J. R. and E. F. Plechaty (1986) TART and ALICE Input Manual, UCID-17026, Lawrence Livermore National Laboratory, Livermore, CA.

7. Plechaty, E. F. and D. E. Cullen (1976) Resonance Self-Shielding Calculations Using the Probability Table Method, UCID-17230, Lawrence Livermore National Laboratory, Livermore, CA

8. Lewis, F. H. and P. D. Soran (1978) "Calculations of UH_3 Critical Masses for Various Uranium Enrichments," Nucl. Sci. and Eng., 68 (1): 116.

9. Brandon, D. I. (1986), Personal communication.

10. Lamarsh, J. R. (1966) Introduction to Nuclear Reactor Theory, Addison-Wesley Publishing Company, Inc.,